Sequential Monte Carlo for States and Parameters Estimation in Dynamic Thermal Models

Loïc RAILLON, Christian GHIAUS
loic.raillon1@insa-lyon.fr, christian.ghiaus@insa-lyon.fr
Univ Lyon, CNRS, INSA-Lyon, Université Claude Bernard Lyon 1, CETHIL UMR5008, F-69621, Villeurbanne, France

Abstract

Experimental identification of grey box model is the key of two social needs, the energy performance measurement and the energy management. Obtaining a reliable model may be time consuming and depends on the knowledge of building characteristics available. Furthermore, on-site measurements have to be collected before starting the identification process. From these facts, this paper investigates the capabilities of a sequential Monte Carlo method to learning models. An unoccupied house under real weather conditions has been used to test the proposed method. It has been shown that even if the chosen model structure is not the best, the sequentially learnt model provides satisfactory simulation results. Indeed, information on the building were used in the initialization which has prevented the algorithm to diverge from physical meaning. Afterwards, insights from the identified model may be used to improve the model with the complete data set.

Introduction

Building performance modelling is facing two important societal needs: the guarantee of energy performance and the estimation of building energy consumption for facilitating energy demand response.

In many countries, energy consumption estimation is mandatory for obtaining the buildings permits. However, the methods used for energy consumption estimation present a variance of 50% between the estimated and measured values (Turner & Frankel 2008). About 70% of this variance may be explained by the differences between the inputs used for estimation, which are not measured on-site, and those which affect the real building. The energy consumption depends on inputs and therefore cannot be a measure of building energy performance. Building energy performance should be given by the intrinsic thermal characteristics of buildings, i.e. by the physical parameters of thermal models which relate inputs to outputs measured on-site.

The identified model can also be useful to facilitate building energy management. Indeed nowadays, the energy production and storage are adjusted such that the energy demand is always satisfied. The complexity of this strategy will be augmented with the increasing of the share of renewable energy sources in the energy mix. The energy sustainability and the network efficiency can be improved by the demand response, in which the demand is adapted to the production. Building energy demand can be estimated by using model predictive control where the forecast is given by the identified model and predicted inputs.

Solving these two social demands requires breaking the scientific deadlocks 1) of experimental model identification of the building and its systems and 2) of the measurement or estimation of the inputs.

State of the art

The emergence of energy harvesting wireless technology offers a way to make the monitoring of buildings more interoperable. The flow of information is important and it has to be embedded in a model to extract information. The popularization of model predictive control (Afram & Janabi-Sharifi 2014) has increased the focus on model identification because the efficiency of the control strategy depends on the model accuracy. Black box or grey box models are usually employed to describe the system through inputs and outputs. However, grey box models introduce more information since their parameters and structures have a physical meaning. In certain cases, relations between mathematical and physical parameters exist if the black box structure is chosen such that it matches the physical one (Naveros et al. 2015).

Identification of physical parameters of thermal models is not new and a number of outdoor experiments under real weather conditions have proved the capability of the method (Bloem 1994, Jiménez 2014) . Parameters of grey box models are either identified iteratively or sequentially. The former method fits the model on a batch of data whereas the latter updates the model as soon as new information become available. Nonetheless, in both cases, the state estimation is solved sequentially by the Kalman filter or an approximation of it. Different iterative methods have been successfully applied to experiments of various scales (Andersen et al. 2014, Bacher & Madsen 2011, Wang & Xu 2006, Zayane 2011) . Identify a reliable model is time-consuming and depends on the a-priori knowledge of the building. Iterative methods require that the data are available; therefore the monitoring time is not put in good use. Sequential methods can be employed during the monitoring time to provide a first model fit and insightful information.

Unlike iterative methods, sequential methods estimate the states and parameters based only on the most recent data and previous estimation, which make the problem more complex. To estimate simultaneously both states and parameters, the parameters are added to the state vector which transforms a linear problem into a non-linear one. Hence, a Kalman filter approximation is required to solve the problem such as the extended Kalman filter (Fux et al. 2014), the unscented Kalman filter (Maasoumy et al. 2014, Martincevic et al. 2015, Radecki & Hencey 2012) or the ensemble Kalman filter (Huchuk et al. 2014). The main difficulty of this strategy is the tuning of the parameter evolutions. Indeed, the parameters are treated as dynamic variables but they should converge to fixed values to preserve the physical meaning of the thermal model; it is a trade-off between exploring the parameter space and converging. Moreover, the dimension of the state vector rapidly increases with the number of parameters, which makes the initialization and tuning of the algorithm harder. This is why the sequential estimation is usually used for low order models.

This paper provides a method based on sequential Monte Carlo for estimating states and parameters. A description of the test case is given and then the methodology for obtaining the state space representation from the thermal network is outlined. Afterwards, the theoretical development of the proposed method is presented and the capabilities of the proposed method are tested on the real test case.

Test case

The test case considered is the second experiment conducted by Fraunhofer Institute in Holzkirchen (near Munich, Germany) on the twin house O5 during April and May 2014. It is an unoccupied single family house with 100 m^2 ground floor, a cellar and an attic space; a full description is given in Strachan et al. (2016). The ground floor is divided in two, the south (green zone Figure 1) and the north zone.

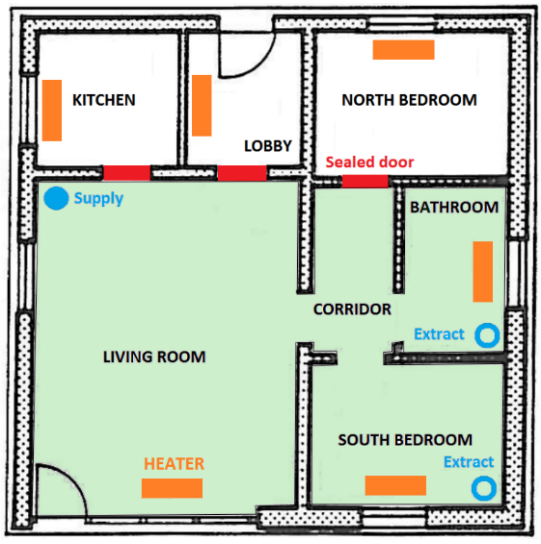

Figure 1: Layout of the house

The cellar, the attic and the north zone are considered as boundary spaces with the air temperature kept constant at 22 °C. However, the air temperatures in the north zone differ from the set-point despite the fact that the blinds were closed and the doors connecting the two zones were sealed to reduce the chance of overheating; only the blinds in the south were opened. Mechanical ventilation was set to supply a volume flow rate of 60 m^3/h into the living room and extract 30 m^3/h in the bathroom and the south bedroom. Electric heaters of the south zone were used with a Randomly Ordered Logarithmic Binary Sequence (ROLBS). The ROLBS signal provides sufficient excitation and maximizes the temperature difference with the outdoor and adjacent spaces. The signal was designed to cover the range of time constants from 1 hour to 90 hours and avoid correlation with solar radiations. Based on these specifications, a model structure for the south zone has to be chosen.

Dynamic thermal model

The south zone is modelled by a third order thermal network (Figure 2) where the thermal transfers through the envelope, the ventilation and the adjacent zone are represented. More precisely the heat transfer rates [W] are defined:

- q_1: infiltration and windows conduction
- q_2: outside air convection
- q_3: wall conduction
- q_4: wall conduction and inside air convection
- q_5: zone wall conduction
- q_6: ventilation advection

The accumulation of energy is represented by the thermal capacities of the wall C_w, of the indoor air with internal walls and furniture C_i, and of the wall separating the two zones C_z. The inputs considered are the following temperature sources [°C] and heat rate sources [W]:

- T_o: outdoor temperature
- T_v: ventilation temperature
- T_z: north zone temperature
- $\dot{Q}_o$: solar radiation on the outside wall surfaces
- $\dot{Q}_i$: solar radiation through the windows
- $\dot{Q}_{HVAC}$: heat flow from HVAC system

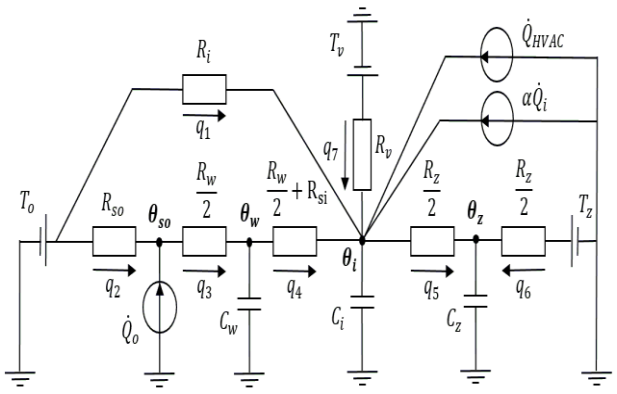

Figure 2: Thermal network of the south zone

Table 1: Information required for modified nodal analysis

Branches $[k_{1:7}]$			**Nodes** $[l_{1:4}]$				
q	G	b	θ				
			θ_{so}	θ_w	θ_i	θ_z	
q_1	$1/R_i$	T_o	0	0	1	0	
q_2	$1/R_{so}$	T_o	1	0	0	0	
q_3	$2/R_w$	0	-1	1	0	0	
q_4	$2/R_w + 2R_{si}$	0	0	-1	1	0	
q_5	$2/R_z$	0	0	0	-1	1	
q_6	$2/R_z$	T_z	0	0	0	1	
q_7	$1/R_v$	T_v	0	0	1	0	
			0	C_w	C_i	C_z	C
			$\dot{Q}_o$	0	$\dot{Q}_{in}$	0	f

The thermal networks in Figure 2 can easily be transformed in state-space representation by using modified nodal analysis; a complete description of the method is given by Ghiaus (2013). All the elements required for building the state space representation are concatenated in Table 1, l and k denoting the number of nodes and branches. The shaded part in Table 1 represents the incidence matrix A, where the rows contain heat rate flow q_k crossing a thermal resistance R_k and the columns contain temperature nodes θ_l. The incidence matrix is filled in row k with -1 if the flow q_k leaves the node, 1 if it enters the node and 0 if the resistance R_k is not connected to the node. The state space is obtained by first writing the heat transfer rates in matrix form

$$e = -A\theta + b \tag{1}$$

$$q = Ge \tag{2}$$

where b is the vector of temperature sources and G is the diagonal matrix of thermal conductivities.

The heat balance in each temperature node is defined by

$$C\dot{\theta} = A^T q + f \tag{3}$$

where $\dot{\theta}$ is the time derivative of θ.

Putting (1) in (2) and then (2) in (3) it results

$$C\dot{\theta} = K\theta + K_b b + f \tag{4}$$

$$K = -A^T G A \tag{5}$$

$$K_b = A^T G \tag{6}$$

where f is the vector of heat rate sources and C is the diagonal matrix of thermal capacities.

All the nodes are not connected to a thermal capacity; therefore the diagonal of the matrix C has zeros and cannot be inverted. This fact is highlighted by writing equation (4) in bloc-matrix form

$$\begin{bmatrix} 0 & 0 \\ 0 & C_c \end{bmatrix} \begin{bmatrix} \dot{\theta}_0 \\ \dot{\theta}_c \end{bmatrix} = \begin{bmatrix} K_{11} & K_{12} \\ K_{21} & K_{22} \end{bmatrix} \begin{bmatrix} \theta_0 \\ \theta_c \end{bmatrix} + \begin{bmatrix} K_{b1} \\ K_{b2} \end{bmatrix} b + \begin{bmatrix} I_{11} & 0 \\ 0 & I_{22} \end{bmatrix} \begin{bmatrix} f_0 \\ f_c \end{bmatrix} \tag{7}$$

where the subscripts c and 0 denote respectively nodes with and without thermal capacities, and I_{11} and I_{22} are identity matrices of appropriate dimensions.

The continuous state space is obtained by eliminating nodes without thermal capacity and therefore separate differential and algebraic equations

$$\dot{\theta}_c = A_s\theta_c + B_s u \tag{8}$$

$$\theta_0 = C_s\theta_c + D_s u \tag{9}$$

with A_s the state matrix,

$$A_s = C_c^{-1}(-K_{21}K_{11}^{-1}K_{12} + K_{22}) \tag{10}$$

B_s the input matrix,

$$B_s = C_c^{-1}[-K_{21}K_{11}^{-1}K_{b1} + K_{b2} \;\; -K_{21}K_{11}^{-1} \;\; I_{22}] \tag{11}$$

C_s the output matrix,

$$C_s = -K_{11}^{-1}K_{12} \tag{12}$$

D_s the feedthrough matrix

$$D_s = -K_{11}^{-1}[K_{b1} \;\; I_{11} \;\; 0] \tag{13}$$

and u the input vector

$$u = [b \; f]^T \tag{14}$$

In this case, the output matrix C_s is chosen by taking the state θ_i as the output, which implies that the feed through matrix is zero. The input vector (14) is given by

$$u = [T_o \; T_o \; 0 \; 0 \; 0 \; T_z \; T_v \; \dot{Q}_o \; 0 \; \dot{Q}_{in} \; 0]^T \tag{15}$$

with $\dot{Q}_{in} = \alpha\dot{Q}_i + \dot{Q}_{HVAC}$.

The input matrix B_s can be reduced by taking only the columns corresponding to non-zero elements in u and by adding the first and the second column of B_s.

The differential algebraic equations (8) and (9) provide a deterministic description of the system but physical systems are often influenced by random disturbances. To describe the deviation between the equations and the true variation of the state, additive noise term is introduced

$$\dot{\theta}_c = A_s\theta_c + B_s u + \sigma\dot{\omega} \tag{16}$$

with σ the scaling of the incremental variance and ω a Wiener process.

The output of the system is observed at discrete time instant $k\Delta t$ e.g. $\theta_{c_k} = \theta_c(k\Delta t)$, therefore the output equation is expressed in discrete time

$$y_k = C_d\theta_{c_k} + v_k \tag{17}$$

where v_k is a white noise process with covariance Σ_v and $C_d = C_s$.

Equations (16) and (17) represent stochastic continuous-discrete system. By assuming a zero-order hold for the

input and equally space data, (16) can be discretized to obtain

$$\theta_{k+1} = A_d \theta_{c_k} + B_d u_k + w_k \tag{18}$$

with w_k a white noise process with covariance Σ_w and

$$A_d = e^{A_s \Delta_t} \tag{19}$$

$$B_d = \int_{\tau=0}^{\Delta_t} e^{A_s \tau} d\tau \, B_s \tag{20}$$

$$\Sigma_w = \int_0^{\Delta_t} e^{A_s \tau} \sigma \sigma^T e^{A_s \tau^T} d\tau \tag{21}$$

Equations (19) and (21) can be computed simultaneously by (Kristensen et al. 2004)

$$exp\left(\begin{bmatrix} -A_s & \sigma\sigma^T \\ 0 & A_s^T \end{bmatrix} \Delta_t\right) = \begin{bmatrix} H_1(\Delta_t) & H_2(\Delta_t) \\ 0 & H_3(\Delta_t) \end{bmatrix} \tag{22}$$

and combining sub matrices of (22)

$$\Sigma_w = H_3^T(\Delta_t) H_2(\Delta_t) \tag{23}$$

$$A_d = H_3^T(\Delta_t) \tag{24}$$

Equation (20) is computed by

$$B_d = A_s^{-1}(A_d - I) B_s \tag{25}$$

However, information in the system (17), (18) are often unknown or not measured and have to be estimated. The next section gives a theoretical development of a Bayesian method for sequentially estimate the states and parameters.

Bayesian estimation

The following discrete state space (with a general enough form to include a large variety of model) is considered

$$x_k = f(x_{k-1}, u_{k-1}, w_{k-1}, z) \tag{26}$$

$$y_k = g(x_k, v_k) \tag{27}$$

where (26) is the state equation, (27) the output equation, $x \in \mathbb{R}^n$ the state, $y \in \mathbb{R}^p$ the output, $u \in \mathbb{R}^m$ the input and $z \in \mathbb{R}^q$ the static parameter. $w \in \mathbb{R}^n$ and $v \in \mathbb{R}^p$ are respectively the process and measurement noise with covariance Σ_w and Σ_v. The subscript k denotes the current time step and $k-1$ the previous one.

Following the notation of Sarkka (2013), the discrete state space (26), (27) can be written in a probabilistic form

$$x_k \sim p(x_k | x_{k-1}, u_{k-1}) \tag{28}$$

$$y_k \sim p(y_k | x_k) \tag{29}$$

with (28) the conditional probability distribution of the current state given the state and input at the previous time step and (29) the conditional probability distribution of the measurement given the state.

The state is assumed to be a Markov sequence, which means that all information about the current state is summarized in the previous state

$$p(x_k | x_{k-1}, u_{k-1}) = p(x_k | x_{1:k-1}, u_{k-1}, y_{1:k-1}) \tag{30}$$

where $y_{1:k-1} = [y_1, y_2, \dots, y_{k-1}]$ denotes a set of data.

Furthermore, the current measurement is independent of the state and measurement history

$$p(y_k | x_k) = p(y_k | x_{1:k}, y_{1:k-1}) \tag{31}$$

Firstly, the static parameter vector z is assumed known and only the state estimation is considered. In a Bayesian sense, the purpose is to construct the marginal posterior distribution of the state $p(x_k | y_k)$. The term posterior refers to the knowledge on the state knowing the measurement and the term marginal refers to the posterior distribution at time k given the history of measurements up to the time k.

Using Bayes' rule and properties (30) and (31), the marginal posterior distribution is given by

$$p(x_k | y_{1:k}) = \frac{p(y_k | x_k) p(x_k | y_{1:k-1})}{p(y_k | y_{1:k-1})} \tag{32}$$

Equation (32) can be computed recursively by first predicting the next state

$$\begin{aligned} &p(x_k | y_{1:k-1}) \\ &= \int p(x_k | x_{k-1}, u_{k-1}) p(x_{k-1} | y_{1:k-1}) dx_{k-1} \end{aligned} \tag{33}$$

and then updating the prediction with the most recent measurement $p(y_k | x_k)$. The normalizing factor in (32) is defined by

$$p(y_k | y_{1:k-1}) = \int p(y_k | x_k) p(x_k | y_{1:k-1}) dx_k \tag{34}$$

For discrete linear and Gaussian state spaces, such as

$$\begin{aligned} &p(x_k | x_{k-1}, u_{k-1}) = \\ &\mathcal{N}(x_k | A_d(z) x_{k-1} + B_d(z) u_{k-1}, \Sigma_w) \end{aligned} \tag{35}$$

$$p(y_k | x_k) = \mathcal{N}(y_k | C_d x_k, \Sigma_v) \tag{36}$$

the integrals (33), (34) can be evaluated in closed form by the Kalman filter (Sarkka 2013). The recursion starts by defining the state prior distribution $p(x_0) \sim \mathcal{N}(m_0, P_0)$, normally distributed with mean m_0 and covariance P_0. The prior distribution represents the knowledge on the state before seeing a measurement. The state prior distribution at time k is

$$p(x_k | y_{1:k-1}) = \mathcal{N}(x_k | m_k^-, P_k^-) \tag{37}$$

with the prior state mean and covariance given by

$$m_k^- = A_d x_{k-1} + B_d u_{k-1} \tag{38}$$

$$P_k^- = A_d P_{k-1} A_d^T + \Sigma_w \tag{39}$$

The one-step predictive distribution for the observation is

$$p(y_k | y_{1:k-1}) = \mathcal{N}(y_k | C_d m_k^-, S_k) \tag{40}$$

where the one-step prediction covariance is defined by

$$S_k = C_d P_k^- C_d^T + \Sigma_v \tag{41}$$

By defining the one-step prediction error

$$e_k = y_k - C_d m_k^- \tag{42}$$

and the Kalman gain

$$K_k = P_k^- C_d^T S_k^{-1} \tag{43}$$

the state prior distribution (37) is updated with the current measurement to form the marginal posterior distribution

$$p(x_k|y_{1:k}) = \mathcal{N}(x_k|m_k, P_k) \tag{44}$$

with the updated mean and covariance

$$m_k = m_k^- + P_k^- C_d^T S_k^{-1} e_k \tag{45}$$

$$P_k = P_k^- - P_k^- C_d^T S_k^{-1} C_d P_k^- \tag{46}$$

The static parameter vector z in (35), (36) is now considered unknown and it has to be estimated simultaneously with the state; the purpose is to construct the joint marginal posterior distribution

$$p(x_k, z|y_{1:k}) = \frac{p(y_k|x_k)p(x_k, z|y_{1:k-1})}{p(y_k|y_{1:k-1}, z)} \tag{47}$$

where the state and parameter are propagated by

$$\begin{aligned} &p(x_k, z|y_{1:k-1}) \\ &= \int p(x_k|x_{k-1}, u_{k-1}, z)p(x_{k-1}, z|y_{1:k-1})dx_{k-1} \end{aligned} \tag{48}$$

and the normalizing factor of (47) is given by

$$p(y_k|y_{1:k-1}, z) = \int p(y_k|x_k)p(x_k, z|y_{1:k-1})dx_k \tag{49}$$

However, the parameter vector doesn't appear linearly in the state space (35), (36), therefore (47) cannot be computed in closed form and approximation of the Kalman filter has to be used, such as the extended Kalman filter or the unscented Kalman filter. But these algorithms are sub-optimal and can perform poorly for high dimensional or strongly non-linear problems. In this cases, Monte Carlo approximation is preferred (Doucet et al. 2001). The main issue in Bayesian estimation is to compute expectations of the form

$$\mathbb{E}[h(x)] = \int h(x)p(x)dx \tag{50}$$

where $p(x)$ is a probability distribution and $h(x)$ is an arbitrary function, for instance the mean value is obtained by $h(x) = x$ (Cappe et al. 2007).

Expectations (50) can be approximated by a set of N random samples $\{x^{(i)}\}_{i=1}^N$ (particles), drawn from a distribution $p(x)$

$$\mathbb{E}[h(x)] \approx \frac{1}{N}\sum_{i=1}^{N} h(x^{(i)}) \tag{51}$$

For the purpose considered here, $p(x)$ is the joint marginal posterior distribution of the state and parameter (47). But it is not possible to sample directly from (47) due to its complicated form. The idea is to use an alternate distribution $q(x)$ (importance distribution) where it is easier to sample from (Chen 2003). The samples are weighted by the importance weights $\omega^{(i)}$ in order to take into account the discrepancy between the posterior distributions (47) and the importance distribution $q(x)$

$$\omega^{(i)} = \frac{p(x^{(i)})}{q(x^{(i)})} \tag{52}$$

Hence, the expectation (51) is given by

$$\mathbb{E}[h(x)] \approx \sum_{i=1}^{N} \omega^{(i)} h(x^{(i)}) \tag{53}$$

The importance weights can be computed sequentially by first writing that (47) is proportional to

$$\begin{aligned} &p(x_k, z|y_{1:k}) \\ &\propto p(y_k|x_k)p(x_k|x_{k-1}, u_{k-1}, z)p(x_{k-1}, z|y_{1:k-1}) \end{aligned} \tag{54}$$

then if the importance distribution $q(x)$ is chosen such that it can be factorized similarly, the importance weights are given by (Cappe et al. 2007)

$$\omega_k^{(i)} \propto \frac{p(y_k|x_k^{(i)})p(x_k^{(i)}|x_{k-1}^{(i)}, u_{k-1}, z^{(i)})}{q(x_k^{(i)}|x_{k-1}^{(i)}, u_{k-1}, z^{(i)}, y_{1:k})}\omega_{k-1}^{(i)} \tag{55}$$

The proportionality in (54) comes from the fact that the normalizing factor (49) has been neglected, therefore the importance weights are only known up to a normalizing constant and have to be normalized

$$\omega_n^{(i)} = \frac{\omega^{(i)}}{\sum_{i=1}^N \omega^{(i)}} \tag{56}$$

A particle approximation of the joint marginal posterior distribution (47) is obtained by sampling from the importance distribution $q(x)$ and then updating the weights with (55). However this method suffers from particle degeneracy (Doucet et al. 2001), which means that all the particles have a negligible weight; thus the posterior distribution is approximated only by a few particles. This problem is solved by using a resampling step, where the particles with small weights are discarded and particles with large weights are duplicated to keep a number of particle constant.

This method is efficient if a sufficient number of particles generated from the importance distribution are in high probability region of the posterior distribution. A popular choice of importance distribution is the state transition distribution (28), which leads to the bootstrap filter (Gordon et al. 1993) but an optimal choice is the one that minimizes the variance of the importance weights

$$\begin{aligned} &q(x_k^{(i)}|x_{k-1}^{(i)}, u_{k-1}, z^{(i)}, y_k) \\ &= \frac{p(y_k|x_k^{(i)})p(x_k^{(i)}|x_{k-1}^{(i)}, u_{k-1}, z^{(i)})}{p(y_k|x_{k-1}^{(i)}, z^{(i)})} \end{aligned} \tag{57}$$

Using (57) in (55), the importance weights are computed by

$$\omega_k^{(i)} \propto p(y_k|x_{k-1}^{(i)}, z^{(i)})\, \omega_{k-1}^{(i)} \tag{58}$$

Hence the particles are resampled according to the predictive likelihood $p(y_k|x_{k-1}, z)$ which means that, the particles will be propagated in high probability region of the state space. The optimal importance distribution (57) is available only when the process and measurement noise

are additive white noises and the output equation is linear (Arulampalam et al. 2002); which is the case for the model (35), (36). The efficiency of the method can be further improved by exploiting the linear Gaussian substructure of the model (35), (36). Thanks to the Bayes' theorem, the joint marginal posterior distribution can be split such that

$$p(x_k, z|y_{1:k}) = p(x_k|z, y_{1:k})p(z|y_{1:k}) \quad (59)$$

therefore the state posterior distribution can be integrated out using the Kalman filter (Schön & Gustafsson 2003). This technic provides better estimates because the dimension of $p(z|y_{1:k})$ is smaller than $p(x_k, z|y_{1:k})$, so the particles represent a lower dimensional space and the estimation of $p(x_k|z, y_{1:k})$ by the Kalman filter is optimal.

As mentioned in the second section, the parameters evolution has to be specified. A common strategy is to add an artificial dynamic (Kantas et al. 2015)

$$z_k = z_{k-1} + w_{z_{k-1}} \quad (60)$$

where $w_{z_{k-1}} \sim \mathcal{N}(0, \Sigma_z)$ is a white noise process with decreasing variance. The time step subscript in the parameter notation helps to distinguish values between two time steps and doesn't represent time varying parameters. However, this strategy requires a significant amount of tuning to perform satisfactory. To overcome these issues, the kernel density method (Liu & West 2001) can be employed. The marginal posterior distribution of the parameters (59) is approximated by a mixture of Gaussian distributions

$$p(z_k|y_{1:k}) \approx \sum_{i=1}^{N} \omega_k^{(i)} \mathcal{N}(z_k^{(i)}|\eta_k^{(i)}, h^2 V_{k-1}) \quad (61)$$

with $\omega_k^{(i)}$ the importance weights and η_k the kernel location given by

$$\eta_k^{(i)} = a z_{k-1}^{(i)} + (1-a)\bar{z}_{k-1} \quad (62)$$

and the constant a controls the shrinkage of the particles toward the Monte Carlo mean $\bar{z}$

$$\bar{z}_{k-1} = \sum_{i=1}^{N} \omega_{k-1}^{(i)} z_{k-1}^{(i)} \quad (63)$$

The particles are propagated according to the Monte Carlo variance

$$V_{k-1} = \sum_{i=1}^{N} \omega_{k-1}^{(i)} (z_{k-1}^{(i)} - \bar{z}_{k-1})(z_{k-1}^{(i)} - \bar{z}_{k-1})^T \quad (64)$$

where the constant h controls the degree of particles dispersion. The constants a and h are determined by $h^2 = 1 - (\frac{3\delta-1}{2\delta})^2$ and $a = \sqrt{1-h^2}$ where δ is usually chosen between 0.95 and 0.99 (Liu & West 2001). The Monte Carlo variance (64) decreases over time because the particles are slightly pushed toward their overall mean and because the particles are resampled. The kernel density method is employed with a resample-propagate scheme; the particles are resampled according to the predictive likelihood (58), such that only promising particles are propagated. The sequential algorithm for estimating the states and parameters for the state space (35), (36) is given in Algorithm 1. This algorithm has been evaluated in simulation but the results are not presented here due to the limited size of the paper; only the results on a real test case are presented in the next section.

Algorithm 1

1. Kernel location

$$\bar{z}_{k-1} = \sum_{i=1}^{N} \omega_{k-1}^{(i)} z_{k-1}^{(i)}$$

$$\eta_k^{(i)} = a z_{k-1}^{(i)} + (1-a)\bar{z}_{k-1}$$

$$V_{k-1} = \sum_{i=1}^{N} \omega_{k-1}^{(i)} (z_{k-1}^{(i)} - \bar{z}_{k-1})(z_{k-1}^{(i)} - \bar{z}_{k-1})^T$$

2. Compute importance weights

$$e_k = y_k - C_d\left(A_d(\eta_k^{(i)}) x_{k-1}^{(i)} + B_d(\eta_k^{(i)}) u_{k-1}\right)$$

$$S_k^{(i)} = C_d\left(A_d(\eta_k^{(i)}) P_{k-1}^{(i)} A_d(\eta_k^{(i)})^T + \Sigma_w\right) C_d^T + \Sigma_v$$

$$\omega_{log}{}_k^{(i)} \propto -\frac{1}{2} log\left(|S_k^{(i)}|\right) - \frac{1}{2} e_k^{T(i)} S_k^{-1(i)} e_k^{(i)}$$

3. Normalize the importance weights

$$\omega_k^{(i)} = e^{\left(\omega_{log}{}_k^{(i)} - max\left(\omega_{log}{}_k^{(i)}\right)\right)}$$

$$\omega_{n_k}^{(i)} = \frac{\omega_k^{(i)}}{\sum_{i=1}^{N} \omega_k^{(i)}}$$

4. Resample

Sample indices $\{k_1, k_2, \ldots, K_N\}$ from $i = \{1,2,\ldots,N\}$ with probabilities $\omega_{n_k}^{(i)}$

5. Propagate parameters

$$z_k^{(i)} \sim \mathcal{N}(\eta_k^{(k_i)}, h^2 V_{k-1})$$

6. Kalman filter prediction

$$m_k^{-(i)} = A_d(z_k^{(i)}) m_{k-1}^{(ki)} + B_d(z_k^{(i)}) u_{k-1}$$

$$P_k^{-(i)} = A_d(z_k^{(i)}) P_{k-1}^{(k_i)} A_d(z_k^{(i)})^T + \Sigma_w$$

7. Kalman filter measurement update

$$S_k^{(i)} = C_d P_k^{-(i)} C_d^T + \Sigma_v$$

$$m_k^{(i)} = m_k^{-(i)} + P_k^{-(i)} C_d^T S_k^{-1(i)} (y_k - C_d m_k^{-(i)})$$

$$P_k^{(i)} = P_k^{-(i)} - P_k^{-(i)} C_d^T S_k^{-1(i)} C_d P_k^{-(i)}$$

Test case

Each room in the south zone was monitored with three temperature sensors at 10 cm, 110 cm and 170 cm from the ground to measure the stratification of the air. The discrepancy between the three heights is important and almost 4 °C separate the top and the bottom. Each space has been chosen to be the average of the three heights and the south zone temperature θ_i (output) is computed as the average of the different spaces (living room, south bedroom, corridor and bathroom, Figure 1) weighted by their respective volumes; the same method is used for the north zone T_z (kitchen, lobby and north bedroom, Figure 1). The air temperature supplied by the ventilation T_v is also used as an input because the air supplied is warmer than the outdoor air temperature T_o. The solar radiations on the outside wall surfaces $\dot{Q}_o$, and through the windows $\dot{Q}_i$ are the sum of the measured vertical solar radiations multiplied by the corresponding wall and window surfaces. The heating in the south zone is done by three electric heaters; therefore $\dot{Q}_{HVAC}$ is chosen as the sum of their emitted powers. All the measured data used for the sequential estimation of the states and parameters are shown in Figure 3. The data set is 14 days long with 1 hour sampling time. The first plot in Figure 3 contains the temperatures [°C] of, from top to bottom, the south zone θ_i, the north zone T_z, the ventilation T_v and the outdoor T_o. The second plot in Figure 3 is the power supplied by the electric heaters $\dot{Q}_{HVAC}$ [kW] and the third plot contains the solar radiations [kW] received on the outside wall surfaces $\dot{Q}_o$, and through the windows $\dot{Q}_i$.

The south zone temperature is relatively high to maximize the temperature difference with the outdoor and the adjacent spaces; this is not an issue since the building is unoccupied.

The building characteristics given by Strachan et al. (2016) are used to define the prior distributions of the parameters (Table 2).

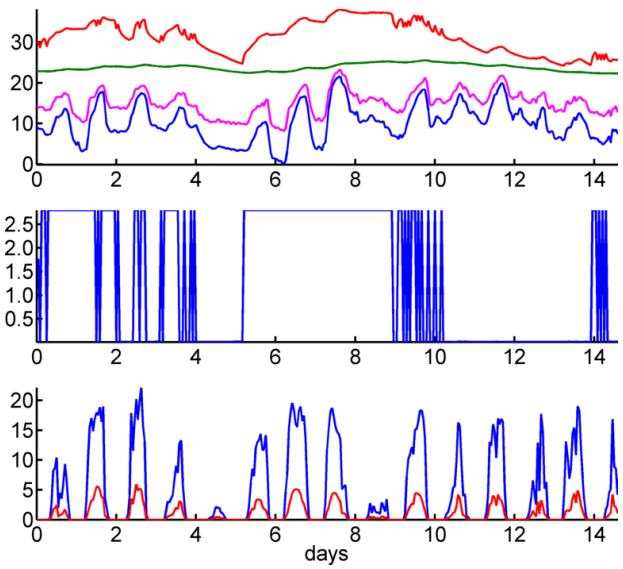

Figure 3: Measured data for identification

The total thermal capacity of the envelope is the sum of the thermal capacities of the n wall of m levels of insulation

$$C_w = \sum_{j=1}^{n}\sum_{i=1}^{m} \rho_i c_i \delta_i S_j = 1.30^7 \text{ J/K} \quad (65)$$

where ρ [kg/m^3] is the density, δ [m] is the thickness, c [J/kg K] is the specific heat and S [m^2] is the wall surface.

Similarly, the thermal resistance of the envelope is

$$R_w = \left(\sum_{j=1}^{n}\left(\sum_{i=1}^{m}\frac{\delta_i}{\lambda_i S_j}\right)^{-1}\right)^{-1} = 9.04^{-2} \text{ K/W} \quad (66)$$

where λ is the conductivity [W/m K].

The thermal resistance of the infiltrations is computed from the pressurization test at 50 Pa

$$R_i = \left(\frac{\rho_a c_a N_{ach} V}{3600}\right)^{-1} = 1.30^{-2} \text{ K/W} \quad (67)$$

where ρ_a and c_a are the density and the specific heat of the air, N_{ach} is the number of air changes per hour and V is the volume of the south zone.

This test indicates infiltration rates not only through the envelope but also through the adjacent zone and boundaries; therefore the air change rate is expected to be lower for the south zone only. The air flow rate of the ventilation is constant and fixed at 60 m^3/h. The air temperature of the ventilation and the indoor air temperature are measured; therefore the heat transfer rate due to mass flow $\dot{m}_v$ introduced into the south zone is

$$q_v = \dot{m}_v c_a (T_v - \theta_i) = \rho_a \frac{60}{3600} c_a (T_v - \theta_i) \quad (68)$$

Thus, the resistance R_v is fixed to

$$R_v = \left(\rho_a \frac{60}{3600} c_a\right)^{-1} = 4.98^{-2} \text{ K/W} \quad (69)$$

The resistance and the thermal capacity of the wall separating the two zones are respectively

$$R_z = \frac{1}{R_{wi_1}} + \frac{3}{R_{door}} + \frac{1}{R_{wi_2}} = 1.34^{-2} \text{ K/W} \quad (70)$$

$$C_z = C_{wi_1} + 3C_{door} + C_{wi_2} = 3.86^6 \text{ J/K} \quad (71)$$

with the subscripts wi_1 and wi_2 denoting respectively the south wall of the living room and the south wall of corridor and bathroom.

The indoor capacity includes the air and the inner walls

$$C_i = \rho_a c_a V + C_{iw_1} + C_{iw_2} = 6.21^6 \text{ J/K} \quad (72)$$

where the subscripts iw_1 and iw_2 correspond respectively to the east wall of the living room and the other light walls. The air temperature in the attic and the cellar is relatively constant, therefore the interactions with these boundaries have been neglected. However, a part of the ceiling and the ground floor capacity has to be taken into account

into C_i. The ground and the ceiling thermal capacities are computed similarly to (65) and the boundary thermal capacity is defined by

$$C_b = C_g + C_c = 7.40^7 \text{ J/K} \tag{73}$$

Hence, the indoor capacity can be reasonably expected to be between (72) and (72) plus the half of (73).

The outdoor and indoor air convection resistances are determined as follow

$$R_{so} = \left(\sum_{j=1}^{n} h_{so} S_j \right)^{-1} = 1.07^{-3} \text{ K/W} \tag{74}$$

$$R_{si} = \left(\sum_{j=1}^{n} h_{si} S_j \right)^{-1} = 7.14^{-3} \text{ K/W} \tag{75}$$

with $h_{so} = 20$ and $h_{si} = 3$ the outside and inside heat convection coefficients $[\text{W/m}^2\text{K}]$.

The thermal resistance of the envelope is defined by

$$R_T = \left(\sum_{j=1}^{n} \left(\frac{1}{h_{so}} + \frac{1}{h_{so}} + \sum_{i=1}^{m} \frac{\delta_i}{\lambda_i} \right)^{-1} \right)^{-1} \tag{76}$$

By using the same material properties as in (66), $h_{si} = 3$ and $h_{so} = 20$, the thermal resistance of the envelope equals to $R_t = 1.54 \text{ m}^2.\text{K/W}$. It is assumed that the convection coefficients can take values between $h_{so} = [4\,, 24]$ and $h_{si} = [2\,, 8]$. The use of these lower and upper values in (76), introduces respectively a variation of 8.08% and -4.79% w.r.t $R_t = 1.54 \text{ m}^2.\text{K/W}$. Therefore, it seems reasonable to fix these parameters instead of increasing the parameters space.

The prior distributions of the parameters were chosen to be normally distributed with means and standard deviations given in Table 2 and shown in Figure 4. The prior distributions represent the knowledge and confidence on the initial parameter values. The measurement and process noises are not estimated but instead fixed and assumed to be small because the hourly data used are averages of data of one minute sampling time. The process and measurement covariance are directly tune in discrete time with the following values

$$\Sigma_w = \begin{pmatrix} 10^{-3} & 0 & 0 \\ 0 & 10^{-3} & 0 \\ 0 & 0 & 10^{-3} \end{pmatrix} \tag{77}$$

$$\Sigma_v = 10^{-4} \tag{78}$$

The prior distribution of state is defined with the respective state mean and covariance

$$\theta_0 = [19 \quad 29.84 \quad 27]^T \tag{79}$$

$$P_0 = \begin{pmatrix} 0.5^2 & 0 & 0 \\ 0 & 0.05^2 & 0 \\ 0 & 0 & 0.5^2 \end{pmatrix} \tag{80}$$

The previous measurement has been used to initialize the value of θ_i in (79).

Table 2: Mean and 3 standard deviations of the prior and posterior distributions of the parameters

	Prior		**Posterior**	
	mean	**3 σ**	**mean**	**3 σ**
R_i	5.00^{-2}	2.10^{-2}	3.49^{-2}	6.42^{-4}
R_w	9.00^{-2}	9.00^{-3}	9.23^{-2}	2.27^{-4}
R_z	1.30^{-2}	2.70^{-3}	1.12^{-2}	1.30^{-4}
α	3.50^{-1}	9.00^{-2}	3.51^{-1}	2.19^{-3}
C_w	1.30^7	1.50^6	1.23^7	7.57^4
C_i	1.50^7	3.00^6	1.70^7	4.61^4
C_z	3.90^6	2.10^5	3.80^6	8.46^3

The discount factor of the kernel density method (61) has been set to $\delta = 0.9$ and a number of $N = 2000$ particles has been used. The estimated states are shown in Figure 5 where the estimated south zone temperature θ_i follows precisely the measurement, both signals cannot be distinguished in the plot. The estimated states stay in a physical range but the wall temperature θ_w contains fast variations due to switching sequence of the heaters which are not present in the wall separating the south and north zone θ_z; this is unlikely because the thermal capacity C_z is smaller than C_w.

The parameters posterior distributions are plotted in Figure 4 and their properties are given in Table 2. The standard deviations of the posterior distributions are considerably smaller than the prior distributions (Figure 4). However, the posterior distributions are included in the prior distributions which can indicate a good initialization or a lack of exploration in the parameters space. Consequently, the estimated parameters belong to the physical range used to initialize the algorithm.

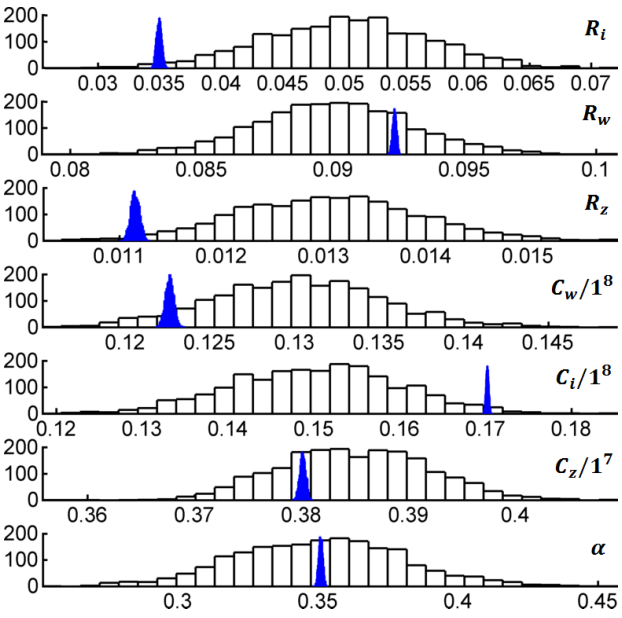

Figure 4: Prior (white) and posterior (blue) distributions of the parameters

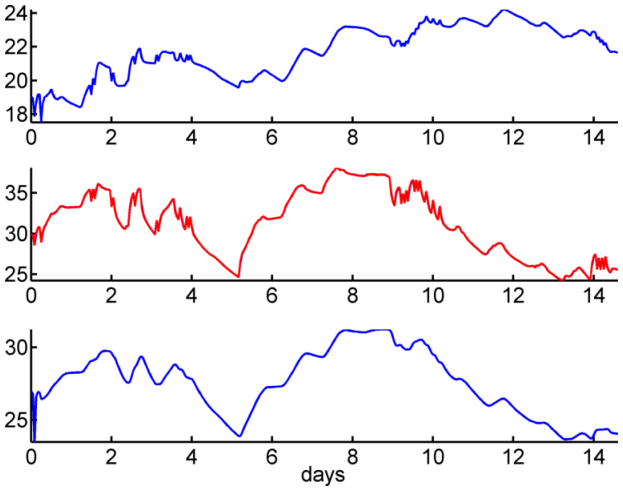

Figure 5: Estimated states, top to bottom: wall θ_w, south zone θ_i (estimated and measured) and boundary wall θ_z

A new data set, starting right after the identification data set (Figure 3) has been used to test the simulation capabilities of the sequentially learnt model. The inputs introduced in the model are shown in Figure 6 and the simulated output distribution of the south zone temperature is compared to the measured one in Figure 7. The order of the signals in Figure 6 is the same as in Figure 3 without the south zone temperature. The model simulation gives satisfactory results: the measured south zone temperature is often contained in the simulated output distribution of the model. Nonetheless, the model is not able to explain the fast variations, especially when the heaters switch on at the beginning of the simulation data set. A one-step prediction error analysis has been used to check the validity of the model. The Kalman filter has been run on the identification data set with the parameters fixed to the posterior mean distribution (Table 2) in order to obtain the one-step prediction error (42).

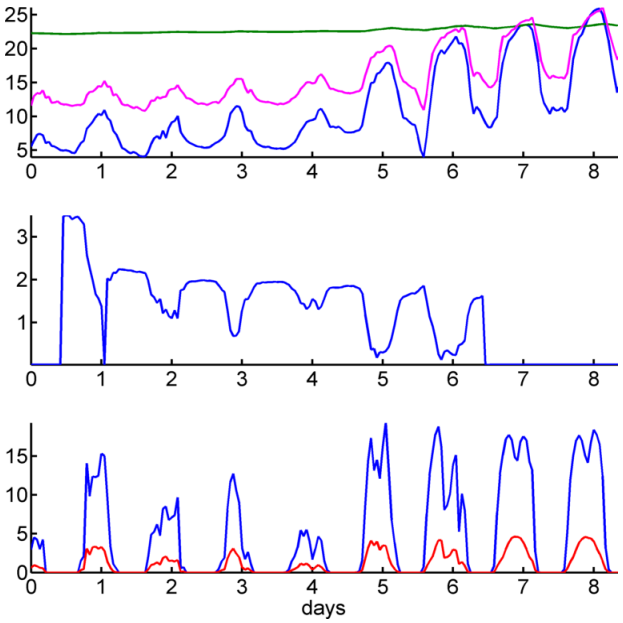

Figure 6: Measured data for simulation

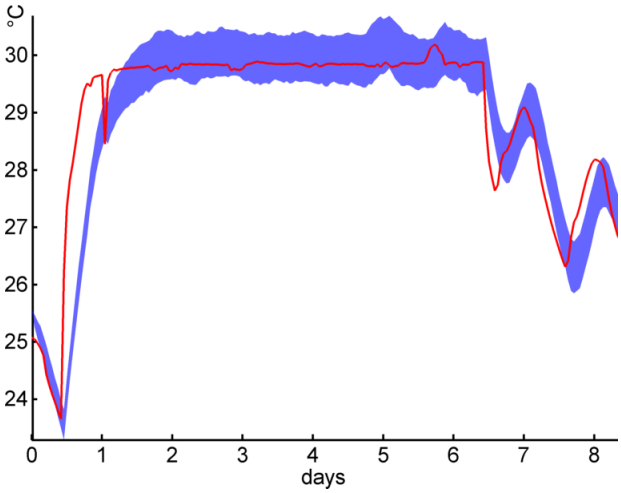

Figure 7: Simulated output distribution (blue) and measured south zone temperature

The autocorrelation function and the cumulated periodogram test have shown that the one-step prediction error is not white noise which means that a better model structure has to be chosen (Madsen 2007). Furthermore, the one-step prediction error is correlated with the heating and the solar radiations, which means that the model is not fully able to explain these input-output relationships. This explains the discrepancy between the simulated and measured temperature (Figure 7) when the heaters switch on.

Conclusion

Experimental identification of grey box models may be time consuming and requires to first collect the data, therefore the monitoring time is not put in good use. This paper has investigated the capabilities of learning models sequentially with a method based on sequential Monte Carlo. The proposed algorithm has been tested on an unoccupied building under real weather conditions. The algorithm was initialized with the buildings characteristics and two weeks of data were used to learn the model. The estimated states and parameters are located in likely physical ranges; however the model validation tests indicate that a better model structure may be chosen. Indeed, the identified model is not able to properly interpret the internal gains. Despite this fact, the simulation capabilities of the identified model are relatively satisfactory and this is mostly due to the physical knowledge introduced in the model. Even if the sequentially learnt model failed the validation tests, it succeeds to provide insights for model refinements with the full data set.

Acknowledgement

This work was financially supported by BPI France in the FUI Project COMETE.

References

Afram, A. & Janabi-Sharifi, F., 2014. Theory and applications of HVAC control systems - A review of model predictive control (MPC). *Building and Environment*, 72, pp.343–355.

Andersen, P.D. et al., 2014. Characterization of heat dynamics of an arctic low-energy house with floor heating. *Building Simulation*, 7(6), pp.595–614.

Arulampalam, M.S. et al., 2002. A Tutorial on Particle Filters for Online Nonlinear / Non-Gaussian Bayesian Tracking. , 50(2), pp.174–188.

Bacher, P. & Madsen, H., 2011. Identifying suitable models for the heat dynamics of buildings. *Energy and Buildings*, 43(7), pp.1511–1522. Available at: http://dx.doi.org/10.1016/j.enbuild.2011.02.005.

Bloem, J.., 1994. Institute for Systems Engineering a N D Informatics Workshop on Application of System Identification.

Cappe, O., Godsill, S.J. & Moulines, E., 2007. An Overview of Existing Methods and Recent Advances in Sequential Monte Carlo. *Proceedings of the IEEE*, 95(5), pp.899–924. Available at: http://www.irisa.fr/aspi/legland/ref/cappe07a.pdf.

Chen, Z.H.E., 2003. Bayesian Filtering: From Kalman Filters to Particle Filters, and Beyond. *Statistics*, 182(1), pp.1–69. Available at: http://citeseerx.ist.psu.edu/viewdoc/download?doi=10.1.1.107.7415&rep=rep1&type=pdf.

Doucet, A., de Freitas, N. & Gordon, N., 2001. An Introduction to Sequential Monte Carlo Methods. *Sequential; Monte Carlo Methods in Practice*, pp.3–14. Available at: http://link.springer.com/chapter/10.1007/978-1-4757-3437-9_1.

Fux, S.F. et al., 2014. EKF based self-adaptive thermal model for a passive house. *Energy and Buildings*, 68, pp.811–817. Available at: http://linkinghub.elsevier.com/retrieve/pii/S0378778812003039 [Accessed December 22, 2014].

Ghiaus, C., 2013. Causality issue in the heat balance method for calculating the design heating and cooling load. *Energy*, 50, pp.292–301. Available at: http://linkinghub.elsevier.com/retrieve/pii/S0360544212007864 [Accessed January 7, 2015].

Gordon, N.J., Salmond, D.J. & Smith, a. F.M., 1993. Novel approach to nonlinear/non-Gaussian Bayesian state estimation. *IEE Proceedings F Radar and Signal Processing*, 140(2), p.107.

Huchuk, B., Cruickshank, C.A. & Gunay, H.B., 2014. Recursive thermal building model training using Ensemble Kalman Filters. *eSim 2014 Conference, Ottawa, Canada, May 7-10*, pp.1–11.

Jiménez, M.J., 2014. *Reliable building energy performance characterisation based on full scale dynamic measurements*,

Kantas, N. et al., 2015. On Particle Methods for Parameter Estimation in General State-Space Models. *Statistical Science*, 30(3), pp.328–351.

Kristensen, N.R., Madsen, H. & Jørgensen, S.B., 2004. Parameter estimation in stochastic grey-box models. *Automatica*, 40(2), pp.225–237.

Liu, J. & West, M., 2001. Combined Parameter and State Estimation in Simulation-based Filtering. *Sequential Monte Carlo Methods in Practice*, pp.197–223. Available at: http://link.springer.com/chapter/10.1007/978-1-4757-3437-9_10.

Maasoumy, M. et al., 2014. Handling model uncertainty in model predictive control for energy efficient buildings. *Energy and Buildings*, 77, pp.377–392. Available at: http://linkinghub.elsevier.com/retrieve/pii/S0378778814002771 [Accessed October 29, 2014].

Madsen, H., 2007. *Time series analysis*,

Martincevic, A., Starcic, A. & Vasak, M., 2015. Parameter estimation for low-order models of complex buildings. *IEEE PES Innovative Smart Grid Technologies Conference Europe*, 2015–Janua(January).

Naveros, I. et al., 2015. Physical parameters identification of walls using ARX models obtained by deduction. *Energy and Buildings*, 108, pp.317–329.

Radecki, P. & Hencey, B., 2012. Online Building Thermal Parameter Estimation via Unscented Kalman Filtering. , pp.3056–3062.

Sarkka, S., 2013. Bayesian Filtering and Smoothing. *Cambridge University Press*, p.254. Available at: http://dl.acm.org/citation.cfm?id=2534502%5Cnhttp://ebooks.cambridge.org/ref/id/CBO9781139344203.

Schön, T. & Gustafsson, F., 2003. particle filters for system identification of state-space models linear in either parameters or states. *Journal of Chemical Information and Modeling*, 53(9), pp.1689–1699.

Strachan, P. et al., 2016. *Empirical Whole Model Validation Modelling Specification Validation of Building Energy Simulation Tools*,

Turner, C. & Frankel, M., 2008. Energy Performance of LEED ® for New Construction Buildings. *New Buildings Institute*, pp.1–46.

Wang, S. & Xu, X., 2006. Simplified building model for transient thermal performance estimation using GA-based parameter identification. *International Journal of Thermal Sciences*, 45(4), pp.419–432. Available at: http://linkinghub.elsevier.com/retrieve/pii/S1290072905001614 [Accessed January 5, 2015].

Zayane, 2011. *Identification d 'un modèle de comportement thermique de bâtiment à partir de sa courbe de charge*.